minerals

MDPI

Article

$[Au(CN)_2]$—Adsorption on a Graphite (0001) Surface: A First Principles Study

Xianhai Li [1,2,3,4], Qin Zhang [2,3,4,*], Jun Xie [2,3,4,5] and Zhihui Shen [2,3,4]

1 College of Materials and Metallurgy, Guizhou University, Guiyang 550025, China; xhli1@gzu.edu.cn
2 Mining College, Guizhou University, Guiyang 550025, China; junx198910@163.com (J.X.); shen_zh9009@163.com (Z.S.)
3 National & Local Joint Laboratory of Engineering for Effective Utilization of Regional Mineral Resources from Karst Areas, Guiyang 550025, China
4 Guizhou Key Lab of Comprehensive Utilization of Non-Metallic Mineral Resources, Guiyang 550025, China
5 College of Resources and Environmental Engineering, Guizhou University, Guiyang 550025, China
* Correspondence: zq6736@163.com; Tel.: +86-851-8829-2081

Received: 2 August 2018; Accepted: 25 September 2018; Published: 27 September 2018

Abstract: Gold is mainly present in the form of $[Au(CN)_2]^-$ during the cyanide leaching process, and this $[Au(CN)_2]^-$ can be adsorbed by graphite in carbonaceous gold ore resulting in preg-robbing gold. In order to clarify the adsorption mechanism between the $[Au(CN)_2]^-$ and graphite, the interaction between the $[Au(CN)_2]^-$ and graphite (0001) surface was studied using density functional theory (DFT). The distance between $[Au(CN)_2]^-$ and graphite (0001) decreased from (4.298–4.440 Å) to (3.123–3.343 Å) after optimization, and the shape of $[Au(CN)_2]^-$ and graphite (0001) obviously changed from straight to curved, which indicated that the $[Au(CN)_2]^-$ had been adsorbed on the graphite (0001) surface. A partial densities of state (PDOS) analysis revealed that there was little change in the delocalization and locality of the PDOS on the graphite (0001) surface after adsorption. However, the valence bands of the Au 5d orbital, C 2p orbital, and N 2p orbital near the Fermi level moved slightly towards lower energy levels; therefore, the adsorption configuration was stable. An analysis of the Mulliken charge population indicated that the Au, N, and C in $[Au(CN)_2]^-$ obtained 0.26, 0.18, 0.04 electrons after adsorption, respectively, while C(surf) lost 0.03 electrons. $[Au(CN)_2]^-$ changed to a conductor from an insulator after adsorption. Taking into account the surface electrical properties of $[Au(CN)_2]^-$ and graphite (0001), there was still a slight electrostatic adsorption between them. The analysis of adsorption energy, electronic structure, PDOS, electron density, Mulliken charge population, and Mulliken bond population revealed that $[Au(CN)_2]^-$ could be adsorbed to the graphite (0001) surface; the adsorption was a type of physical adsorption (including electrostatic adsorption) and mainly occurred on the two C≡N. These results contributed to the understanding of the mechanisms involved in preg-robbing gold formation by graphite and the optimization of this process during cyanide leaching.

Keywords: graphite (0001); $[Au(CN)_2]^-$; adsorption; CASTEP codes; first principles

1. Introduction

Fine grain disseminated gold ore (FGDGO) deposits are the most important gold deposits in the world and are mainly distributed in Nevada in the United States, and in the two "golden triangle" regions of Yunnan, Guizhou, and Guangxi, and Sichuan, Shanxi, and Gansu provinces in China [1–3], in which carbonaceous matter is widespread. Apart from carbonates, carbonaceous matter in gold ores mainly includes elemental carbon, organic carbon, hydrocarbons, and other biological matters, and elemental carbon is graphite or amorphous carbon [4–7]. Carbonaceous gold ore is a kind of

refractory gold ore resource, the processing of which is impacted by "preg-robbing" behavior and the inhibition of Au dissolution by carbonaceous matter [4,8–10]. Cyanide has always been the preferred complexing agent in the leaching of gold ore, even though there are many other complexing agents, because the cyanide has a higher chemical stability, lower cost, and better understood chemistry than other agents [11–14]. Gold in the ore slurry reacts with cyanide according to the following chemical reaction [3,15–17]:

$$4Au_{(s)} + 8CN^-{}_{(aq)} + O_{2(g)} + 2H_2O_{(l)} <=> 4[Au(CN)_2]^-{}_{(aq)} + 4OH^-{}_{(aq)} \quad (1)$$

Au might exist within the $[Au(CN)_2]^-$ structure during the cyanide leaching process; therefore, research into the adsorption of $[Au(CN)_2]^-$ and graphite is important to determine the adsorption mechanism of carbonaceous matter and to improve the gold leaching rate in gold ore leaching.

A number of previous studies investigated the interaction between substances and graphite using first-principles. Sha et al. [18] investigated the interaction between H atoms and a graphite (0001) surface based on spin-polarized density functional theory using the generalized gradient approximation and ultrasoft pseudopotentials. Perea-Ramirez et al. [19] studied the adsorption of radicals obtained from catechol and guaiacol derivatives on a graphite surface through a theoretical analysis in the context of the electro-grafting process. He et al. [20] used first-principles methods to systematically investigate the electronic density of states, work function, and adsorption energy of methane molecules adsorbed on graphite (0001) films. However, there have been few systematic studies of the adsorption between $[Au(CN)_2]^-$ and the surface of graphite. Therefore, the mechanism of the adsorption of $[Au(CN)_2]^-$ to the graphite surface remains to be studied.

Calculations based on the first-principles method can investigate the adsorption structure and adsorption mechanism from the atomic level [21–26]. Computational modelling is a powerful method for researching physical–chemical phenomena, and has been extensively used in plenty of fields in recent years, such as mining, hydrometallurgy, the chemical industry, materials, and so on [27–30]. Many scientists prefer alternatives, like the Cambridge Serial Total Energy Package (CASTEP) code, to finish calculations based on first principles [29,31,32]. Liu et al. [30] discussed the bulk properties of bcc Fe and graphite and its surface, the work of adhesion, and the electronic structure of the Fe (110)/graphite (0001) interface using CASTEP codes. Wu et al. [33] studied the first-principles calculation of the hexyl thiolate monolayer on Au (111) using CASTEP codes. Wang et al. [34] investigated the adsorption of water molecules on quartz (001) surfaces using CASTEP codes.

The abovementioned studies provide ways to study the adsorption mechanism between $[Au(CN)_2]^-$ and graphite surface using CASTEP codes. This may be the most effective and simple method, since the $[Au(CN)_2]^-$/graphite (0001) interface has not been completely explored and the experiments are difficult to conduct. In this paper, calculations are employed to systematically discuss the adsorption between $[Au(CN)_2]^-$ and graphite (0001) using CASTEP codes based on the first principles.

2. Model and Calculations

2.1. Computational Method

The original graphite units were founded and optimized by the CASTEP of the Material Studio (MS) software based on density functional theory (DFT) [22,31]. The interactions between the ionic core and valence electrons were described using ultra-soft pseudopotential [35]. The K point of the Brillouin region was $1 \times 1 \times 2$ and the energy cutoff was 380 eV [36]. The improved approximation of PW91 by generalized gradient approximation (GGA) was adopted as the exchange correlation function, because it has a high degree of accuracy for the calculation of hydrogen bonding adsorption and chemical adsorption [37,38]. The DFT method alone was not accurate enough to calculate the adsorption between graphite and $[Au(CN)_2]^-$, because the interactions

between them were weak; therefore, the DFT calculation needed to be revised by DFT-D in which the Ortmann–Bechstedt–Schmidt (OBS) correction was adopted [39]. In the calculation process, the DFT-D method was used to correct the weak interactions between graphite and $[Au(CN)_2]^-$, which included Van Der Waal forces. The Broyden Fletcher Goldfarb Shanno (BFGS) method was used to conduct geometric optimization [40]. The optimized convergence parameters were as follows: the energy was 2.0×10^{-5} eV/atom, the maximum displacement was 0.02 Å, the maximum force was 0.5 eV/Å, the maximum stress was 0.1 GPa, and the self-consistent iterative convergence accuracy was 2.0×10^{-6} eV/atom. The vacuum thickness and surface layers of the graphite were tested with the same precision level. The optimization parameters of the gold–dicyanide complex $[Au(CN)_2]^-$ were the same as for the original unit optimization. The atomic orbitals involved in this calculation are as shown in Table 1.

Table 1. The atomic orbitals involved in the calculation.

Elements	Atomic Orbitals
H	$1s^1$
C	$2s^2 2p^2$
N	$2s^2 2p^3$
Au	$5d^{10} 6s^1$

2.2. Computational Models

The model of the graphite unit was taken from the American mineralogical crystal structure database (AMCSD), and the representative graphite structure was adopted (see Figure 1) for the study. Graphite is a layered structure with carbon layer planes parallel to each other. The carbon atoms are arranged in a hexagonal and two-dimensional shape with an interval of 0.335 nm, and the layers are combined by Van der Waals forces. In graphite crystal, the carbon atoms of the same layer form a covalent bond by sp^2 hybrids, in which each atom is bonded to three other atoms to form a hexagonal network. The length of the C–C bonds is 142 pm, which is in accordance with the bond length range of atomic crystal. As a result, each layer is an atomic crystal. The carbon atoms also have a p orbital in the same plane, and they overlap each other. The electrons are free, like free electrons in metals; therefore, graphite is also classified as a metal crystal [30,41]. The graphite (0001) surface is the basal plane, which is predominately exposed in graphite crystal; therefore, the graphite (0001) surface has primarily been used for adsorption studies [20].

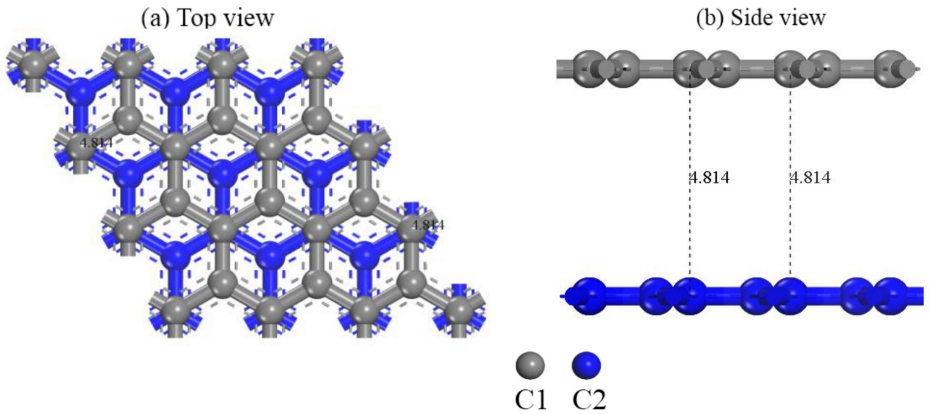

Figure 1. Optimized configuration of graphite before optimization.

In this paper, an ideal graphite crystal model without defects was used, and we selected six hexagons composed of carbon atoms as repeating units to represent graphite (0001) surfaces, and the distance between adjacent carbons on the graphite base was 142 pm. The optimized graphite configuration is shown in the labelled zone of Figure 1. The configuration of the graphite surface after

optimization is shown in Figure 2. After optimization, the distance between carbon atoms in the same layer showed no obvious change; however, the distance between neighboring layers increased from 0.34 nm to 0.48 nm, which indicated that there were stronger interactions between carbon atoms in the same layer, but weaker interactions between carbon atoms in neighboring layers.

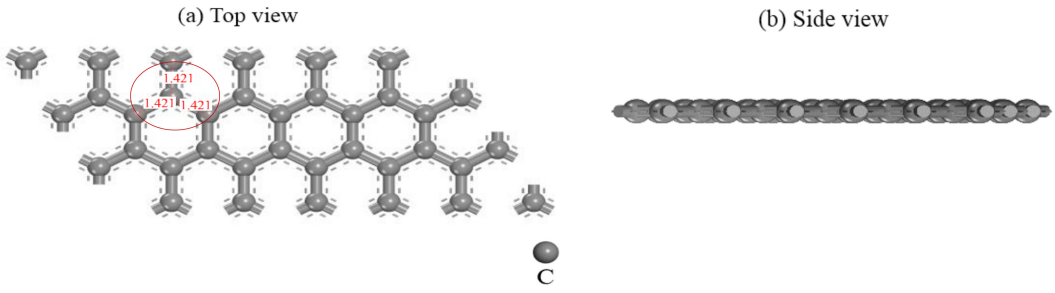

Figure 2. Configuration of the graphite surface after optimization.

By comparing the $[Au(CN)_2]^-$ configuration before and after optimization (see Figure 3), we observed that the molecular shape was always linear, and the C–Au bond length grew weakly, while the C≡N bond length increased more, which indicated that the interactions between the C and N atoms on the surface became weaker.

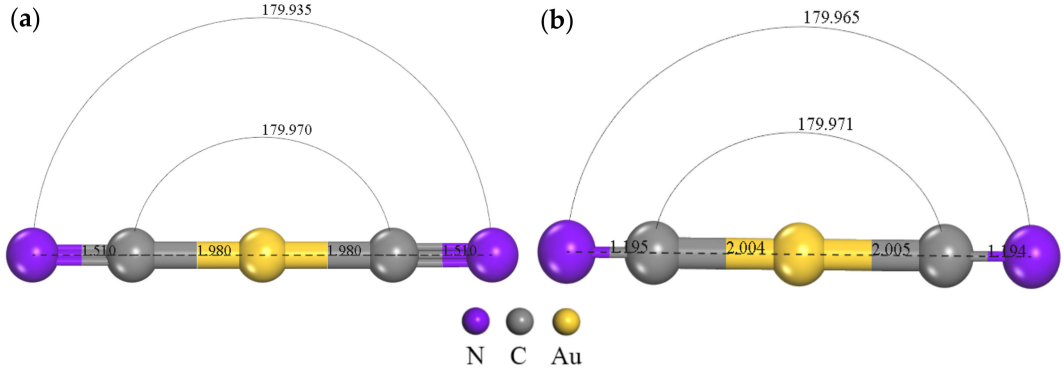

Figure 3. $[Au(CN)_2]^-$ configuration: (**a**) before optimization, (**b**) after optimization.

3. Results and Discussion

3.1. Adsorption Configuration Analysis of $[Au(CN)_2]^-$ on Graphite (0001) Surface

The gold leaching agent NaCN and the Au element can form a stable complex $[Au(CN)_2]^-$ during gold leaching [42,43]. Tan et al. [5] proposed that $[Au(CN)_2]^-$ could be adsorbed by graphite resulting in the loss of gold, called "preg-robbing". The configuration of $[Au(CN)_2]^-$ and the graphite (0001) surface was optimized by the DFT method, and the initial and optimized configurations of $[Au(CN)_2]^-$ and graphite (0001) surface are shown in Figure 4. We can see that the distance between $[Au(CN)_2]^-$ and graphite (0001) reduced to (3.123–3.343 Å) from (4.298–4.440 Å), and $[Au(CN)_2]^-$ was able to form a stable adsorption configuration on the graphite (0001) surface. The angles between N≡C–Au atoms decreased to (172.811°, 173.569°) from (179.547°, 179.641°), the bond length of C≡N decreased to 1.188 Å from 1.195 Å, and the shape of $[Au(CN)_2]^-$ obviously changed to a curved type from a straight line, which indicated that the graphite (0001) surface had been adsorbed by $[Au(CN)_2]^-$, and that the adsorption mainly occurred in the two C≡N. Meanwhile, the center of the graphite (0001) surface was depressed, and the angle was reduced to 178.430° from 180°, which indicated that the graphite (0001) surface had been adsorbed by $[Au(CN)_2]^-$. The calculation results based on DFT showed that the adsorption energy between $[Au(CN)_2]^-$ and the graphite (0001) surface was −48.55 KJ/mol, which indicated that strong physical adsorption had occurred (including slight electrostatic adsorption) [22,44,45]. These results are in agreement with previous studies in which

there was a consensus that the adsorption of $[Au(CN)_2]^-$ onto carbon occurs without chemical changes [11,46]. Meanwhile, the adsorption type was the same as that between activated carbon and $[Au(CN)_2]^-$ according to previous studies [47,48].

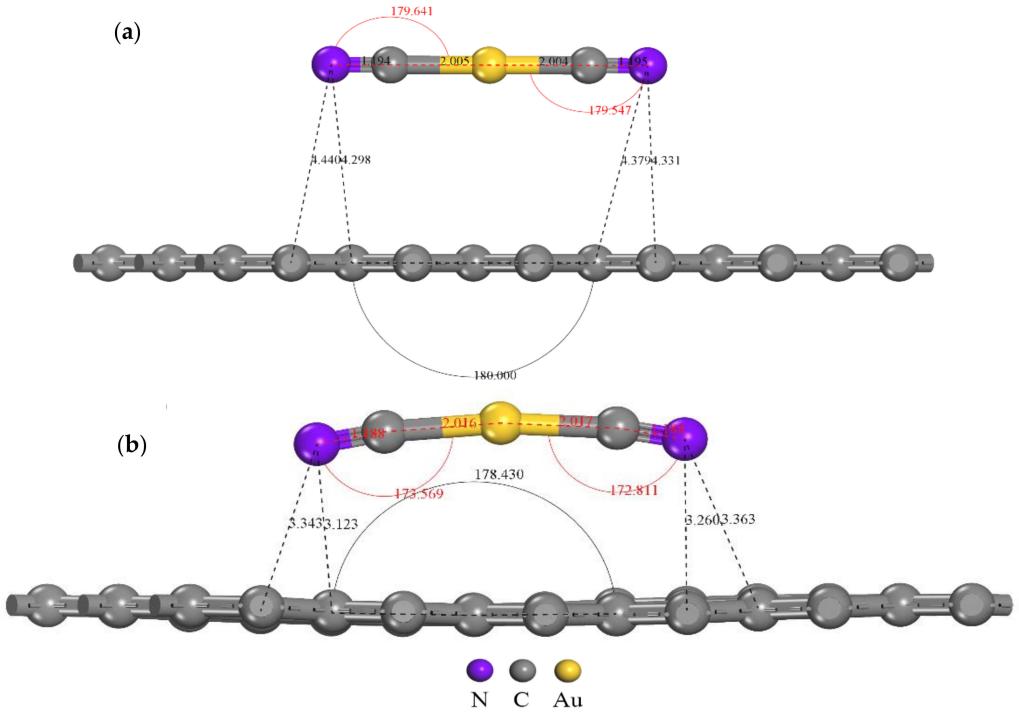

Figure 4. Adsorption configuration: (**a**) initial adsorption configuration, (**b**) optimized adsorption configuration.

3.2. Electronic Structure Analysis of Gold Cyanide on Graphite (0001) Surface

In order to further research the adsorption mechanism of $[Au(CN)_2]^-$ on the graphite (0001) surface, the partial densities of state (PDOS) of graphite (0001) surface and $[Au(CN)_2]^-$ before and after adsorption (see Figure 5a,b), the charge density of the stable adsorption configuration (see Figure 6a), and charge density difference (see Figure 6b) were analyzed.

(**a**)

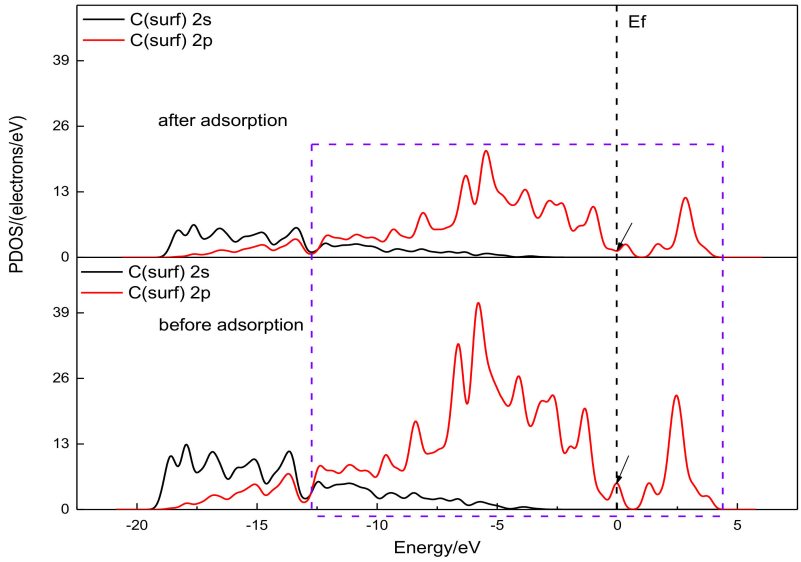

Figure 5. *Cont.*

(**b**)

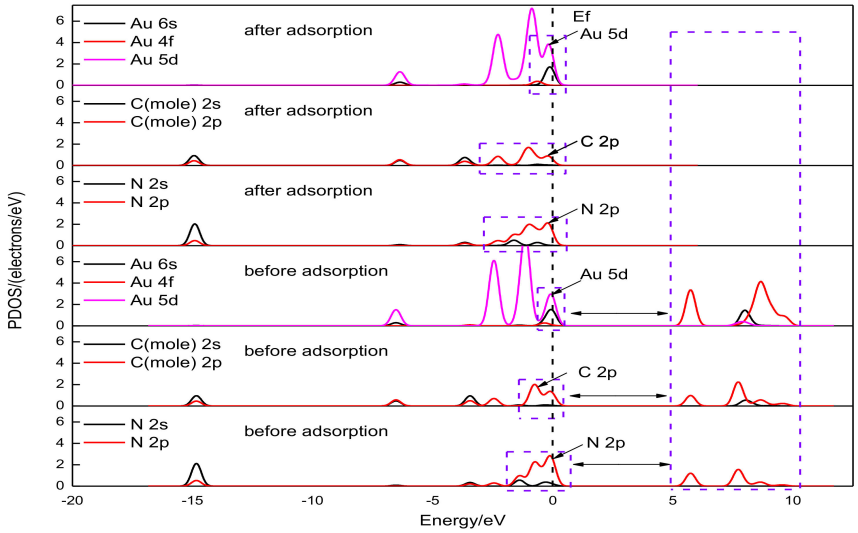

Figure 5. Partial density of state (PDOS) of each atom in graphite (0001) and $[Au(CN)_2]^-$ before and after adsorption. (**a**) PDOS of graphite (0001) before and after adsorption. (**b**) PDOS of each atom in $[Au(CN)_2]^-$ before and after adsorption.

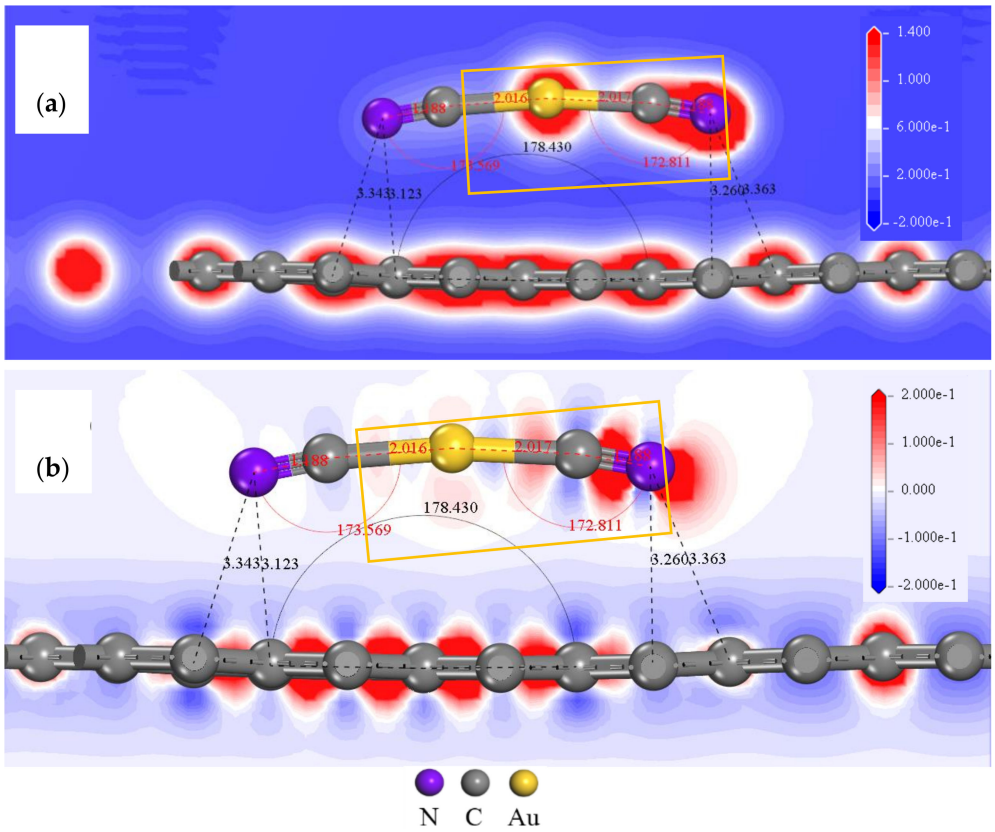

Figure 6. Charge density of the graphite stable adsorption configuration: (**a**) electron density, (**b**) electron density difference.

C(surf) 2p orbital in graphite (0001) crossed the Fermi level (as shown in the arrow in Figure 5a) with a bandwidth of 0, indicating that graphite was a typical conductor, which is consistent with the properties of graphite [49,50]. There was little change in the delocalization and locality of the PDOS on the graphite (0001) surface after adsorption because of the reduction in the density of states (DOS) of the 2s and 2p orbitals in the C(surf) atom. Meanwhile, the sp^3 hybrid orbitals still existed in the C(surf) atom on the graphite (0001) surface, which indicates that the graphite (0001) surface was still

stable. The PDOS of each atom in $[Au(CN)_2]^-$ before and after adsorption varied greatly. This was mainly demonstrated by the following two aspects: on one hand, the valence band densities of the Au, C, and N atoms near the Fermi level moved slightly towards lower energy levels, mainly in the Au 5d orbital, C 2p orbital, and N 2p orbital (as shown by the black arrow in Figure 5b), which resulted in a lower total energy level and a more stable system in $[Au(CN)_2]^-$. On the other hand, the bandwidth of the valence band and the conduction bands of the Au, C, and N atoms were around 5 eV before adsorption (as shown by the blue arrow in Figure 5b). This shows that $[Au(CN)_2]^-$ is a typical insulator before adsorption, which is based on the results of DOS and band structure (bandwidth is about 5 eV), and whether the $[Au(CN)_2]^-$ is an insulator during cyanidation in the practical leaching system requires further verification in future research. After adsorption, the PDOS of the conduction bands of the Au, C, and N atoms disappeared. The Au 5d orbital, the C 2p orbital, and the N 2p orbital directly crossed the Fermi level. The bandwidth became 0 eV, and $[Au(CN)_2]^-$ became a conductor. A possible reason for the conductivity change of $[Au(CN)_2]^-$ might be the formation of adsorption between $[Au(CN)_2]^-$ and the graphite (0001) surface, and the properties of graphite may have had an influence on the conductivity of $[Au(CN)_2]^-$. Based on the above analysis, the changes in PDOS of the Au, C, and N atoms indirectly indicate that $[Au(CN)_2]^-$ was adsorbed on the graphite (0001) surface. In the stable configuration after adsorption, the distance between $[Au(CN)_2]^-$ and the graphite (0001) surface was (3.123–3.343 Å), and the distance between them was far greater than covalent bond length (the covalent bond length is equal to the sum of the equivalent covalency radius of two atoms). In regard to the Mulliken bond population analysis (see Table 2), all atoms in $[Au(CN)_2]^-$ did not bond with C(surf) atoms in graphite (0001). Therefore, the adsorption between $[Au(CN)_2]^-$ and the graphite (0001) surface was physical adsorption, and this result is in agreement with the energy results (−48.55 KJ/mol).

Table 2. Mulliken bonding population of atoms before and after $[Au(CN)_2]^-$ adsorption to the graphite (0001) surface.

Adsorption Model	Bond	Adsorption Status	Population	Length (Å)
Gra–$[Au(CN)_2]^-$	C–N	Before	1.61	1.194
		After	1.71	1.187
	C–Au	Before	0.46	2.004
		After	0.52	2.016
	C(surf)–C(surf)	Before	1.08	1.420
		After	(1.06~1.11)	(1.413~1.424)

The charge density at the Au, C, and N atom sites in $[Au(CN)_2]^-$ became higher after adsorption, as well as in the middle of the graphite (0001) surface (as shown in the marked area in Figure 6a). The higher the charge density, the stronger the physical and chemical activity, and the chemical reactions or adsorption took place more easily, which provides further evidence that the adsorption is mainly concentrated in the two C≡N, as shown in the adsorption configuration analysis. On the whole, $[Au(CN)_2]^-$ had a negative charge. Actually, the Au atom is the center of positive charge in $[Au(CN)_2]^-$, while the N atom is the center of negative charge (as shown in the marked area in Figure 6b). As shown in Figure 6a,b there was charge transfer between the graphite (0001) surface and $[Au(CN)_2]^-$, and the charge was mainly transferred from the graphite (0001) surface to $[Au(CN)_2]^-$. Charge transfer led to the graphite (0001) surface having a positive charge and $[Au(CN)_2]^-$ having a partial negative charge; therefore, there was a certain electrostatic attraction between them which still belonged to the category of physical adsorption

3.3. Mulliken Population Analysis of $[Au(CN)_2]^-$ on the Graphite (0001) Surface

The Au, N, and C in the $[Au(CN)_2]^-$ obtained 0.26, 0.18, 0.04 electrons after adsorption, respectively (see Table 3), while C(surf) lost 0.03 electrons. The electron gain and loss were basically

conserved between $[Au(CN)_2]^-$ and the graphite (0001) surface in terms of the atom number, which led to partial negative charge of the $[Au(CN)_2]^-$ and positive charge of the graphite (0001) surface. The results are in agreement with the results of the charge density and differential charge density analyses. The 6s orbital and the 5d orbital in the Au atom mainly obtained electrons, the 2p orbital in the N atom mainly obtained electrons, the 2p orbital in C mainly obtained electrons, and the 2p orbital in C(surf) on the graphite (0001) surface mainly lost electrons. The activity of orbitals gaining and losing electrons was stronger near the Fermi level (shown in the markup area in Figure 5b).

Table 3. Mulliken charge population of atoms before and after $[Au(CN)_2]^-$ adsorption to the graphite (0001) surface.

Adsorption Model	Atom Name	Adsorption Status	Valence Electrons Number					Charge (e)
			s	p	d	f	Total	
Gra–$[Au(CN)_2]^-$	Au	Before	0.87	0.00	9.42	0.08	10.37	0.63
		After	1.04	0.00	9.56	0.03	10.63	0.37
	N	Before	1.74	3.53	0.00	0.00	5.27	–0.26
		After	1.72	3.73	0.00	0.00	5.45	–0.46
	C	Before	1.29	2.77	0.00	0.00	4.06	−0.05
		After	1.28	2.81	0.00	0.00	4.09	–0.09
	C(surf)	Before	1.05	2.95	0.00	0.00	4.00	0.00
		After	1.05	2.92	0.00	0.00	3.97	0.03

The length of the C≡N bond was 1.194 Å and the population was 1.61; the length of C–Au in $[Au(CN)_2]^-$ was 2.004 Å and the population was 0.46 before adsorption (see Table 2). Meanwhile, the length of the C≡N bond was 1.187 Å, and the population was 1.71, and the length of C–Au in $[Au(CN)_2]^-$ was 2.016 Å and the population was 0.52 after adsorption. The Mulliken bond population analysis showed that when the bond length was shorter, and the population was bigger, the covalency was stronger. Therefore, the covalency of C≡N and C–Au were both enhanced; although the C–Au bond length became longer, the population value increased and covalency increased. The population values were 1.08 and 1.06~1.11 on the graphite (0001) surface before and after adsorption, respectively. The local covalency of C(surf)–C(surf) became stronger, which provides further evidence for the adsorption of $[Au(CN)_2]^-$ and C(surf) atoms in the graphite (0001) surface, as shown in the configuration analysis.

Although the covalency of C≡N, C–Au, and C(surf)–C(surf) changed, there were no bands between the each atom in $[Au(CN)_2]^-$ and the C(surf) atoms in graphite (0001); therefore, there was no chemical adsorption between them, which is in agreement with the adsorption configuration and calculation of adsorption energy. Although no chemical bonds formed between $[Au(CN)_2]^-$ and C(surf) atoms in graphite (0001), the adsorption between the $[Au(CN)_2]^-$ and C(surf) atoms in graphite (0001) definitely exists, and is shown by the downward bending of $[Au(CN)_2]^-$ and the upward bending of the graphite (0001). At the same time, it was also shown, from another angle, that the type of adsorption between them was physical adsorption. The adsorption energy between $[Au(CN)_2]^-$ and graphite (0001) surface was −48.55 KJ/mol, which indicated that it was physical adsorption between $[Au(CN)_2]^-$ and the graphite (0001) surface.

Based on the above research, it can be concluded that $[Au(CN)_2]^-$ can be adsorbed on graphite (0001) surfaces by physical adsorption rather than chemical adsorption, providing a basis for preg-robbing gold by graphite in gold leaching. Considering that preg-robbing gold in the leaching process is a very complex process (including preg-robbing gold by organic carbon, preg-robbing gold by activated carbon and the interference of other chemicals in pulp), it should be studied further.

4. Conclusions

The interaction between $[Au(CN)_2]^-$ and the graphite (0001) surface was studied by DFT. The adsorption configuration analysis showed that $[Au(CN)_2]^-$ forms stable adsorption configurations on graphite (0001) of the physical adsorption type (including electrostatic adsorption).

After $[Au(CN)_2]^-$ adsorption on the graphite (0001) surface, the shape of $[Au(CN)_2]^-$ obviously changed to a curved type, the distance between $[Au(CN)_2]^-$ and the graphite (0001) surface reduced, and the angles between the N≡C–Au atoms decreased, which indicated that adsorption between $[Au(CN)_2]^-$ and the graphite (0001) surface does exist. The distance between $[Au(CN)_2]^-$ and the graphite (0001) surface was (3.123–3.343 Å) after adsorption, which is far greater than the distance of chemisorption. Therefore, the adsorption was physical adsorption, which is in agreement with the level of adsorptive energy (−48.55 KJ/mol). $[Au(CN)_2]^-$ changed from an insulator to a conductor after adsorption due to $[Au(CN)_2]^-$ adsorption on the graphite (0001) surface, which indicates that the conductivity of graphite might affect the $[Au(CN)_2]^-$ during the adsorption process. The activity of the gain and loss of electrons in each orbital was stronger near the Fermi level (Au, N, and C in $[Au(CN)_2]^-$ obtained 0.26, 0.18, and 0.04 electrons after adsorption, respectively, while C(surf) lost 0.03 electrons), which indicated that the adsorption was physical adsorption (including electrostatic adsorption).

The results of the PDOS showed that there was little change in the delocalization and locality of the PDOS on the graphite (0001) surface after adsorption; however, the valence band density of the Au, C, and N atoms near the Fermi level moved slightly towards a lower energy level, mainly in the Au 5d orbital, C 2p orbital, and N 2p orbital, which suggests that the adsorption occurred mainly in the Au 5d orbital, C 2p orbital, and N 2p orbital (C≡N).

It is expected that the present results will be useful to allow researchers to deeply and fundamentally understand the "preg-robbing" behavior of graphite and to optimize the process in the leaching of gold ores.

Author Contributions: X.L. and Q.Z. conceived and designed the computational method and models; Q.Z. contributed the computational resources; X.L. performed the calculations; J.X. and Z.S. helped to analyze the data; X.L. wrote the paper.

Funding: This work was financially supported by the Joint Fund of Guizhou Provincial Department of Science and Technology, China (Project [2014] 7655) and the High-level of Innovative Talents of Guizhou Province, China (Project [2015] 4012).

Conflicts of Interest: The authors declare no conflict of interest.

References

1. Xie, Z.; Xia, Y.; Cline, J.S.; Yan, B.; Wang, Z.; Tan, Q.; Wei, D. Comparison of the native antimony-bearing Paiting gold deposit, Guizhou Province, China, with Carlin-type gold deposits, Nevada, USA. *Miner. Depos.* **2017**, *52*, 69–84. [CrossRef]
2. Muntean, J.L.; Cline, J.S.; Simon, A.C.; Longo, A.A. Magmatic–hydrothermal origin of Nevada's Carlin-type gold deposits. *Nat. Geosci.* **2011**, *4*, 122–127. [CrossRef]
3. Gómez-Díaz, J.; Honkala, K.; López, N. A Density Functional Theory study on gold cyanide interactions: The fundamentals of ore cleaning. *Surf. Sci.* **2010**, *604*, 1552–1557. [CrossRef]
4. Yang, H.; Liu, Q.; Song, X.; Dong, J. Research status of carbonaceous matter in carbonaceous gold ores and bio-oxidation pretreatment. *Trans. Nonferrous Met. Soc. China* **2013**, *23*, 3405–3411. [CrossRef]
5. Tan, H.; Lukey, G.C.; van Devebter, J.S.J. The behaviour of carbonaceous matter in cyanide leaching of gold. *Hydrometallurgy* **2005**, *78*, 226–235. [CrossRef]
6. Li, X.; Zhang, Q.; Shen, Z. Study of the Separation of Carbonaceous Matter in Micro-grained Gold Ore in Guizhou Province. *Nonferrous Met. Miner. Process. Sect.* **2016**, *3*, 33–37.
7. Razvozzhaeva, E.A.; Nemerov, V.K.; Spiridonov, A.M.; Prokopchuk, S.I. Carbonaceous substance of the Sukhoi Log gold deposit (East Siberia). *Russ. Geol. Geophys.* **2008**, *49*, 371–377. [CrossRef]
8. Su, W.; Hu, R.; Xia, B.; Liu, Y. Calcite Sm-Nd isochron age of the Shuiyindong Carlin-type gold deposit, Guizhou, China. *Chem. Geol.* **2009**, *258*, 269–274. [CrossRef]

9. Konadu, K.T.; Sasaki, K.; Kaneta, T.; Ofori-Sarpong, G.; Osseo-Asare, K. Bio-modification of carbonaceous matter in gold ores: Model experiments using powdered activated carbon and cell-free spent medium of Phanerochaete chrysosporium. *Hydrometallurgy* **2017**, *168*, 76–83. [CrossRef]
10. Helm, M.M.; Vaughan, J.P.; Staunton, W.P. Evaluation of preg-robbing in goldstrike carbonaceous ore using raman spectroscopy. In Proceedings of the 50th Annual Conference of Metallurgists of CIM, Montreal, QC, Canada, 2–5 October 2011; pp. 595–606.
11. Ofori-Sarpong, G.; Osseo-Asare, K. Preg-robbing of gold from cyanide and non-cyanide complexes: Effect of fungi pretreatment of carbonaceous matter. *Int. J. Miner. Process.* **2013**, *119*, 27–33. [CrossRef]
12. Senanayake, G. Gold leaching in non-cyanide lixiviant systems: Critical issues on fundamentals and applications. *Miner. Eng.* **2004**, *17*, 785–801. [CrossRef]
13. Zhang, H.; Ritchie, I.M.; La Brooy, S.R. The adsorption of gold thiourea complex onto activated carbon. *Hydrometallurgy* **2004**, *72*, 291–301. [CrossRef]
14. Muir, D.M.; Aylmore, M.G. Thiosulphate as an alternative to cyanide for gold processing—Issues and impediments. *Miner. Process. Extr. Metall.* **2004**, *113*, 2–12. [CrossRef]
15. Raphulu, M.C.; Scurrell, M.S. Cyanide leaching of gold catalysts. *Catal. Commun.* **2015**, *67*, 87–89. [CrossRef]
16. Bas, A.D.; Safizadeh, F.; Zhang, W.; Ghali, E.; Yeonuk, C.H.O.I. Active and passive behaviors of gold in cyanide solutions. *Trans. Nonferrous Met. Soc. China* **2015**, *25*, 3442–3453. [CrossRef]
17. Kianinia, Y.; Reza Khalesi, M.; Abdollahy, M.; Hefter, G.; Senanayake, G.; Hnedkovsky, L.; Darban, A.K.; Shahbazi, M. Predicting Cyanide Consumption in Gold Leaching: A Kinetic and Thermodynamic Modeling Approach. *Minerals* **2018**, *8*, 110. [CrossRef]
18. Sha, X.; Jackson, B. First-principles study of the structural and energetic properties of H atoms on a graphite (0001) surface. *Surf. Sci.* **2002**, *496*, 318–330. [CrossRef]
19. Perea-Ramírez, L.I.; Vargas, R.; Domínguez, Z.; Salas-Reyes, M.; Matus, M.H.; Galván, M. Theoretical study of the adsorption of substituted guaiacol and catechol radicals on a graphite surface. *Electrochim. Acta* **2017**, *242*, 66–72. [CrossRef]
20. Man-Chao, H.; Jian, A.Z. Methane adsorption on graphite (0001) films: A first-principles study. *Chin. Phys. B* **2013**, *22*, 452–456.
21. Han, Y.; Liu, W.; Chen, J. DFT simulation of the adsorption of sodium silicate species on kaolinite surfaces. *Appl. Surf. Sci.* **2016**, *370*, 403–409. [CrossRef]
22. Xie, J.; Li, X.; Mao, S.; Li, L.; Ke, B.; Zhang, Q. Effects of structure of fatty acid collectors on the adsorption of fluorapatite (001) surface: A first-principles calculations. *Appl. Surf. Sci.* **2018**, *444*, 699–709. [CrossRef]
23. Han, Y.; Liu, W.; Chen, J.; Han, Y. Adsorption mechanism of hydroxyl calcium on two kaolinite (001) surface. *J. China Coal Soc.* **2016**, *41*, 743–750.
24. Sun, S.P.; Gu, S.; Sun, J.H.; Xia, F.F.; Chen, G.H. First principles investigation of the electronic properties of graphitic carbon nitride with different building block and sheet staggered arrangement. *J. Alloys Compd.* **2018**, *735*, 131–139. [CrossRef]
25. Ancilotto, F.; Toigo, F. First-principles study of potassium adsorption on graphite. *Phys. Rev. B Condens. Matter* **1993**, *47*, 13713–13721. [CrossRef] [PubMed]
26. Yin, X.; Opara, A.; Du, H.; Miller, J.D. Molecular dynamics simulations of metal–cyanide complexes: Fundamental considerations in gold hydrometallurgy. *Hydrometallurgy* **2011**, *106*, 64–70. [CrossRef]
27. Mohammadnejad, S.; Provis, J.L.; van Deventer, J.S.J. Computational modelling of gold complexes using density functional theory. *Comput. Theor. Chem.* **2015**, *1073*, 45–54. [CrossRef]
28. Mohammadnejad, S.; Provis, J.L.; van Deventer, J.S.J. Computational modelling of interactions between gold complexes and silicates. *Comput. Theor. Chem.* **2017**, *1101*, 113–121. [CrossRef]
29. Gao, X.; Jiang, Y.; Zhou, R.; Feng, J. Stability and elastic properties of Y–C binary compounds investigated by first principles calculations. *J. Alloys Compd.* **2014**, *587*, 819–826. [CrossRef]
30. Liu, Y.; Xing, J.; Li, Y.; Sun, L.; Wang, Y. A first principles study of adhesion and electronic structure at Fe (110)/graphite (0001) interface. *Appl. Surf. Sci.* **2017**, *405*, 497–502. [CrossRef]
31. Segall, M.D.; Lindan, P.J.; Probert, M.A.; Pickard, C.J.; Hasnip, P.J.; Clark, S.J.; Payne, M.C. First-Principles Simulation: Ideas, Illustrations and the CASTEP Code. *J. Phys. Condens. Matter* **2002**, *14*, 2717–2744. [CrossRef]
32. Mattsson, A.E.; Schultz, P.A.; Desjarlais, M.P.; Mattsson, T.R.; Leung, K. Designing meaningful density functional theory calculations in materials science—A primer. *Model. Simul. Mater. Sci. Eng.* **2005**, *13*, R1–R31. [CrossRef]

33. Wu, T.; Cao, D.; Wang, X.; Jiao, Z.; Chen, M.; Luo, H.; Zhu, P. First principle calculations of hexyl thiolate monolayer on Au (1 1 1). *Appl. Surf. Sci.* **2015**, *330*, 158–163. [CrossRef]
34. Wang, X.; Zhang, Q.; Li, X.; Ye, J.; Li, L. Structural and Electronic Properties of Different Terminations for Quartz (001) Surfaces as Well as Water Molecule Adsorption on It: A First-Principles Study. *Minerals* **2018**, *8*, 58. [CrossRef]
35. Vanderbilt, D. Soft self-consistent pseudopotentials in a generalized eigenvalue formalism. *Phys. Rev. B* **1990**, *41*, 7892–7895. [CrossRef]
36. Rafailov, P.M.; Maultzsch, J.; Thomsen, C.; Dettlaff-Weglikowska, U.; Roth, S. Kohn Anomaly and Electron–Phonon Interaction at the K-Derived Point of the Brillouin Zone of Metallic Nanotubes. *Nano Lett.* **2009**, *9*, 3343–3348. [CrossRef] [PubMed]
37. Ireta, J.; Neugebauer, J.; Scheffler, M. On the Accuracy of DFT for Describing Hydrogen Bonds: Dependence on the Bond Directionality. *J. Phys. Chem. A* **2004**, *108*, 5692–5698. [CrossRef]
38. Perdew, J.P. Generalized gradient approximations for exchange and correlation: A look backward and forward. *Phys. B Condens. Matter* **1991**, *172*, 1–6. [CrossRef]
39. Ortmann, F.; Bechstedt, F.; Schmidt, W.G. Semiempirical van der Waals correction to the density functional description of solids and molecular structures. *Phys. Rev. B* **2006**, *73*, 205101. [CrossRef]
40. Pfrommer, B.G.; Côté, M.; Louie, S.G.; Cohen, M.L. Relaxation of Crystals with the Quasi-Newton Method. *J. Comput. Phys.* **1997**, *131*, 233–240. [CrossRef]
41. Luo, X.; Fang, C.; Li, X.; Lai, W.; Liang, T. Adsorption behaviors of Cs and I atoms on the graphite surface by the first-principles. *J. Nucl. Mater.* **2013**, *441*, 113–118. [CrossRef]
42. Khosravi, R.; Azizi, A.; Ghaedrahmati, R.; Gupta, V.K.; Agarwal, S. Adsorption of gold from cyanide leaching solution onto activated carbon originating from coconut shell—Optimization, kinetics and equilibrium studies. *J. Ind. Eng. Chem.* **2017**, *54*, 464–471. [CrossRef]
43. Kondos, P.D.; Deschênes, G.; Morrison, R.M. Process optimization studies in gold cyanidation. *Hydrometallurgy* **1995**, *39*, 235–250. [CrossRef]
44. Miller, D.J.; Hong, H.L. An experimental method for determining heat of physical adsorption. *J. Catal.* **1983**, *81*, 281–290. [CrossRef]
45. Levita, G.; Kajita, S.; Righi, M.C. Water adsorption on diamond (111) surfaces: An ab initio study. *Carbon* **2018**, *127*, 533–540. [CrossRef]
46. Sibrell, P.L.; Miller, J.D. Significance of Graphitic Structural Features in Gold Adsorption by Carbon. *Miner. Metall. Process.* **1992**, *9*, 189–195.
47. Yalcin, M.; Arol, A.I. Gold cyanide adsorption characteristics of activated carbon of non-coconut shell origin. *Hydrometallurgy* **2002**, *63*, 201–206. [CrossRef]
48. Wei, H. Studies on the Gold Adsorption of the Coal Based Activated Carbon in the Contained CN Solution. Master's Thesis, Beijing University of Technology, Beijing, China, June 2010; pp. 1–65.
49. Li, S.; Yao, J.; Lin, D. *Graphite*; Chemical Industry Press: Beijing, China, 1991.
50. Xiang, H.U.; Duan, P.; Song, J.; Li, W.; Chen, L.; Bian, X. Study on the influences of ionization region material arrangement on Hall thruster channel discharge characteristics. *Plasma Sci. Technol.* **2018**, *20*, 024008.